chemistry

MDPI

Article

U(VI) Coordination Modes in Complex Uranium Silicates: $Cs[(UO_6)_2(UO_2)_9(Si_2O_7)F]$ and $Rb_2[(PtO_4)(UO_2)_5(Si_2O_7)]$

Evgeny V. Nazarchuk [1], Oleg I. Siidra [1,2,*], Dmitri O. Charkin [3] and Yana G. Tagirova [1]

[1] Department of Crystallography, Saint-Petersburg State University, University Emb. 7/9, 199034 St. Petersburg, Russia
[2] Kola Science Center, Russian Academy of Sciences, Apatity, 184200 Murmansk, Russia
[3] Inorganic Chemistry Division, Chemistry Department, Moscow State University, Vorobievy Gory 1-3, 119991 Moscow, Russia
* Correspondence: o.siidra@spbu.ru

Abstract: Crystals of two new inorganic uranyl silicates, $Cs[(UO_6)_2(UO_2)_9(Si_2O_7)F]$ (**1**) and $Rb_2[(PtO_4)(UO_2)_5(Si_2O_7)]$ (**2**), were produced from melts in evacuated silica tubes. Their structures have been solved by direct methods: **1** is trigonal, *P*-31*c*, a = 10.2040(3), c = 17.1278(5) Å, V = 1544.45(10) Å^3, R_1 = 0.042; **2** is tetragonal, *P*4/*mbm*, a = 16.0400(24), c = 3.9231(6) Å, V = 1009.34(10) Å^3, R_1 = 0.045. **1** is the first example of cation–cation interactions between the uranyl polyhedra in uranyl silicates. Therein, U^{VI} adopts three coordination modes, UO_6 octahedra, UO_6F, and UO_7 pentagonal bipyramids, with the latter sharing common edges to form U_2O_{12} dimers. Three dimers associate into six-membered rings via cation–cation interactions. The structure of **1** can be described as a complex uranyl fluoride silicate framework with channels filled by the U1 atoms and disordered Cs^+ cations. **2** represents a new type of topology never observed before among the structures of uranyl compounds; it is also a first complex uranium platinum oxide. Therein, the UO_6 tetragonal bipyramids share edges to form chains. Five such chains are stitched into a complex ribbon via the silicon polyhedra. The ribbons are connected into a framework by the PtO_4 squares; rubidium atoms are located in the channels of the framework.

Keywords: uranium; silicates; platinates; cation–cation interactions; framework structures

Citation: Nazarchuk, E.V.; Siidra, O.I.; Charkin, D.O.; Tagirova, Y.G. U(VI) Coordination Modes in Complex Uranium Silicates: $Cs[(UO_6)_2(UO_2)_9(Si_2O_7)F]$ and $Rb_2[(PtO_4)(UO_2)_5(Si_2O_7)]$. *Chemistry* **2022**, *4*, 1515–1523. https://doi.org/10.3390/chemistry4040100

Academic Editors: Edwin Charles Constable and Katharina M. Fromm

Received: 23 October 2022
Accepted: 7 November 2022
Published: 10 November 2022

1. Introduction

Silicates of hexavalent uranium are commonly observed in the oxidation zones of uranium deposits [1]; they are assumed to contribute to the migration of uranium in geological media [2]. To date, there are as many as 21 mineral species containing tetra- and/or hexavalent uranium cations and silicate anions [3]. Strong metamictization of mineral samples essentially hinders their studies by diffraction methods [4]. During model experiments on uraninite oxidation, the $KNa_3[(UO_2)_2(Si_4O_{10})_2](H_2O)_4$ compound was found [5]. Thus, it was demonstrated that uranium silicates can form upon the interaction of uranium-containing wastes with the walls of geological repository. An important property of uranium silicates is the possibility of cation exchange, demonstrated on the samples of boltwoodite [6,7] and cuprosklodowskite [8]. It can play an important role in immobilization or, reversely, the release and subsequent migration of fission products, e.g., ^{137}Cs.

In contrast to minerals, synthetic uranium silicates exhibit more diverse structural chemistry due to the larger ranges of experimental conditions and compositions studied; last but not the least, note the ability of the SiO_4 tetrahedra to polymerize into disilicate groups, chains, layers, and frameworks [8–15]. Microporous uranyl silicates are of particular interest as potential absorbents and ion exchangers, as well as molecular sieves [13]. Many of these intriguing compounds have been produced using flux techniques [16,17].

The topological diversity of uranium compounds is underpinned by the relatively non-rigid coordination of hexavalent uranium, as well as varied modes of polyhedra linkage. In the majority of its inorganic compounds, hexavalent uranium forms a uranyl cation coordinated, in its equatorial plane, by four to six ligands [18]. However, cases are known when the coordination of U^{VI} is closer to regular octahedral [19] or a so called "tetraoxide core" is formed [20]. Most commonly, the uranium polyhedra share their equatorial vertices or edges to each other. The cases interactions via the axial oxygen atoms of uranyl cations are very rare [19,21,22].

Among the uranyl compounds with tetrahedral TO_4 cations, silicates form a relatively small but structurally diverse group. Silicates are often isostructural with reported germanates [17], yet the structural chemistry of the former is richer due to the size difference between the GeO_4 and SiO_4 species, the larger condensation degree of silicate tetrahedra, and better size agreement between the Si_2O_7 group and the equatorial edge of the uranium polyhedron [11].

In the current paper, we report two new complex uranyl silicates: $Cs[(UO_6)_2(UO_2)_9(Si_2O_7)F]$ (**1**) and $Rb_2[(PtO_4)(UO_2)_5(Si_2O_7)]$ (**2**).

2. Materials and Methods

2.1. Synthesis

Red crystals of **1** were obtained during a high-temperature synthesis starting from 120 mg U_3O_8 (Vecton, 99.7%), 24 mg of CsCl (Vecton, 99.7%), 24 mg of RbCl (Vecton, 99.7%), 14 mg of SiO_2 (Vecton, 99.7%), and 60 mg of PbO (Vecton, 99.7%). This mixture was transferred to a silica tube; then, 10 µL of HF was added, after which the tube was evacuated and sealed. The tube was heated to 900 °C at a rate of 100 °C/h, soaked for 50 h, and cooled to room temperature at a rate of 10 °C/h.

Red needle crystals of **2** were obtained during a high-temperature synthesis starting from 100 mg U_3O_8 (Vecton, 99.7%), 15 mg of RbCl (Vecton, 99.7%), 14 mg of SiO_2 (Vecton, 99.7%), and 30 mg of PbO (Vecton, 99.7%). This mixture was first placed in a platinum crucible and then transferred to a silica tube, evacuated, and sealed. The tube was heated to 950 °C at a rate of 100 °C/h, soaked for 100 h, and cooled to room temperature at the rate of 5 °C/h.

2.2. Single-Crystal X-Ray Experiments

Single-crystal X-ray data were collected using a Rigaku XtaLAB Synergy-S diffractometer equipped with a PhotonJet-S detector operating with MoKα radiation at 50 kV and 1 mA. A single crystal of each phase was chosen, more than a hemisphere of data was collected with a frame width of 0.5° in ω, and 10 s were spent counting for each frame. The data were integrated and corrected for absorption by applying a multi-scan type model using the Rigaku Oxford Diffraction programs CrysAlis Pro. Tiny needle crystals of 2 are unstable under an X-ray beam.

The structures of **1** and **2** were solved and successfully refined with the use of the SHELX software package [23]. The atom coordinates and thermal displacement parameters for each atom were collected in the corresponding cif files; experimental parameters are provided in Table 1. Unit cell parameters are presented for a temperature of 300 K.

2.3. Elemental Analysis

Semi-quantitative elemental analyses were measured using a field emission scanning electron microprobe (LEO EVO 50) equipped with an Oxford INCA Energy Dispersive X-ray Spectrometer (EDX). EDX data were collected from several crystals of each compound and demonstrate that Pb and Cl were not incorporated, while the presence of all the elements reported has been confirmed.

Table 1. Crystallographic parameters and structure refinement details for $Cs[(UO_6)_2(UO_2)_9(Si_2O_7)F]$ (**1**) and $Rb_2[(PtO_4)(UO_2)_5(Si_2O_7)]$ (**2**).

Compound	1	2
Crystal system	trigonal	tetragonal
Space group	*P*-31*c*	*P*4/*mbm*
a, Å	10.2040(3)	16.040(2)
c, Å	17.1278(5)	3.9231(6)
V, Å^3	1544.45(10)	1009.3(3)
F(000)	2800	1936
Density	7.351	7.815
Radiation, wavelength, Å	MoK_α, 0.71073	
Ranges of *h*, *k*, *l*	$-13 \le h \le 12$, $-13 \le k \le 12$, $-22 \le l \le 21$	$-18 \le h \le 18$, $-18 \le k \le 18$, $-4 \le l \le 4$
Number of reflections	8347	15,047
Number of unique reflections	1093	525
$2\theta_{min}$–$2\theta_{max}$	3.313–27.987	1.79–24.63
R_{int}/R_{sigma}	0.029/0.043	0.029/0.094
R_1 [F > 4σ(F)]/wR_1	0.029/0.053	0.045/0.12
R_2/wR_2	0.039/0.091	0.064/0.13
GOF	1.162	1.151
CCDC	2,214,650	2,214,660

3. Results

$Cs[(UO_6)_2(UO_2)_9(Si_2O_7)F]$ (1). There are three different types of uranyl polyhedra in the structure of **1**: $U1O_6$, $U2O_6F$ and $U3O_7$. The U1 atoms (Figure 1a) are coordinated by six oxygen atoms (2.066(7) Å × 3 and 2.108(7) Å × 3), thus centering slightly distorted octahedra. Hence, U1 does not form the uranyl cation but rather contributes to the anionic part of the structure forming the $[UO_6]^{6-}$ species. The U2 (Figure 1b) and U3 (Figure 1c) form typical uranyl (*Ur*) cations (<U-O_{ap}> = 1.769(7) and 1.799(7) Å, respectively). *Ur*(2) in the equatorial plane is coordinated by four oxygen (<U-O_{eq}> = 2.433 Å) and one fluorine atom to form *Ur*(2)O_4F polyhedra. *Ur*(3) is coordinated by five oxygens (<U-O_{eq}> = 2.359 Å).

One symmetrically independent silicon atom is tetrahedrally coordinated (Figure 1d) with <Si-O> = 1.642 Å. Two SiO_4 tetrahedra share a common O6 oxygen atom to form the Si_2O_7 disilicate group.

The cesium cations are disordered over two partially occupied sites. The bond valence sums (5.70, 5.76, 5.97, 1.17, and 3.70 *v.u.* for U1, U2, U3, Cs1, and Si1 atoms, respectively), calculated using the parameters from [24], correlate well with the formal valences of the atoms.

Two *Ur*(3)O_5 bipyramids share common O2-O2 edges (Figure 1e,f) to form a *Ur*(3)$_2O_8$ dimer. Three such species are linked via O3 vertices to form six-membered rings (Figure 1f) with U1 atom in the center. The O3 vertex comprises, on the one hand, the apical (uranyl) vertex of one *Ur*(3)O_5 and, on the other hand, an equatorial vertex of another *Ur*(3)O_5 polyhedra. In other words, the dimers are linked via the cation–cation interactions. Three *Ur*(2)O_4F species are linked via a common fluoride vertex into a *Ur*(2)$_3O_{12}$F trimer (Figure 1g). Si_2O_7 disilicate groups are attached to *Ur*(2)$_3O_{12}$F moieties along the *c* axis (Figure 1h).

The structure of **1** can be described as a complex uranyl fluoride silicate framework (Figure 2a,b) with channels filled by the U1 atoms and disordered Cs^+ cations. The framework can be split into two blocks (Figure 2c). The *Ur*(3)O_5 species, which are linked via the cation–cation interaction and Si_2O_7 groups, form the blocks designated here as **A** in Figure 2d, wherein the voids are filled by U1 atoms. The *Ur*(2)$_3O_{12}$F groups are arranged in block **B** with large voids occupied by Cs^+ cations (Figure 2e).

$Rb_2[(PtO_4)(UO_2)_5(Si_2O_7)]$ (2). The structure of **2** contains two symmetrically independent U^{6+} cations, which form linear $(UO_2)^{2+}$ uranyl ions with the U^{6+}-O bond lengths of ca. 1.76 Å (Figure 3a,b). The *Ur* ions are coordinated by four oxygen atoms each, arranged in the equatorial planes of the tetragonal bipyramids. The coordination environments of the Si sites are strongly distorted due to the disorder. According to the results of the stable structure solution, the Si ions are coordinated by three oxygen atoms (Figure 3c) at equatorial plane (<Si-O> = 1.548 Å) and by two half occupied oxygen atoms at vertical plane (Si-O = 1.962(1) Å). The former distances are somewhat shorter, while the latter are longer that those expected for the true "$[SiO_5]^{6-}$" species (1.60 Å [25]). Most likely, the true structure contains two equiprobable "up" and "down" orientations of the SiO_4 tetrahedra, forming disordered disilicate groups (note the one-half occupancy of the O7 site); however, all attempts to split the silicon position into two tetrahedral sites did not provide a stable refinement. Compared to germanium, silicon contributes less to the overall scattering dominated by the uranium, platinum, and cesium cations, so its positioning, particularly in partially occupied sites, faces more difficulties and is less precise.

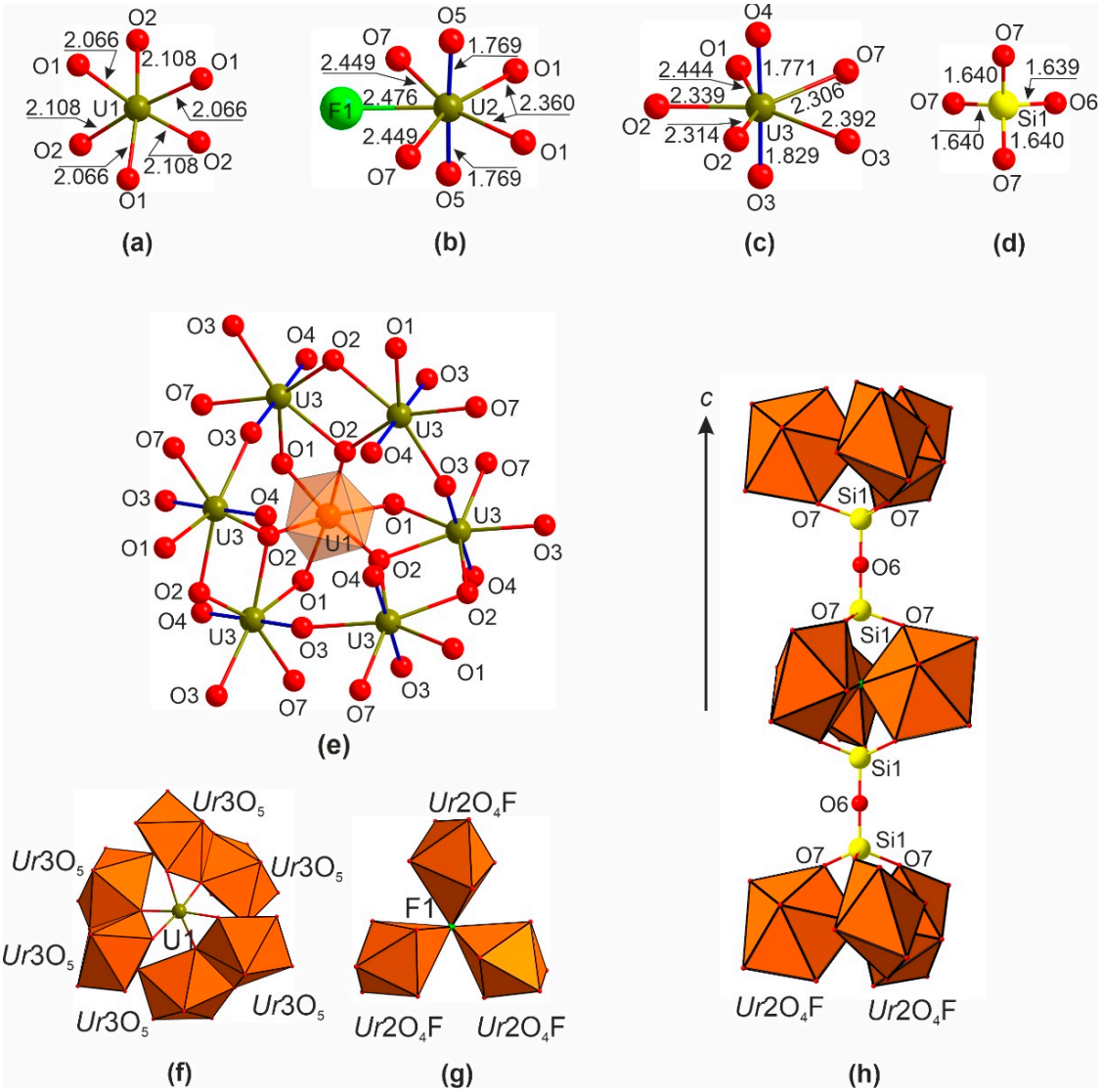

Figure 1. Cation coordination (**a**–**d**) in the structure of $Cs[(UO_6)_2(UO_2)_9(Si_2O_7)F]$. Linkage of the $Ur(3)O_5$ and $U1O_6$ in the ball-and-stick (**e**) and polyhedral representation (**f**) (the uranyl bonds are shown in blue). Linkage of the $Ur(2)O_4F$ polyhedra sharing common F atom in the center thus forming $Ur(2)_3O_{12}F$ trimers (**g**). An arrangement of the Si_2O_7 and $Ur(2)_3O_{12}F$ groups along the *c* axis (**h**).

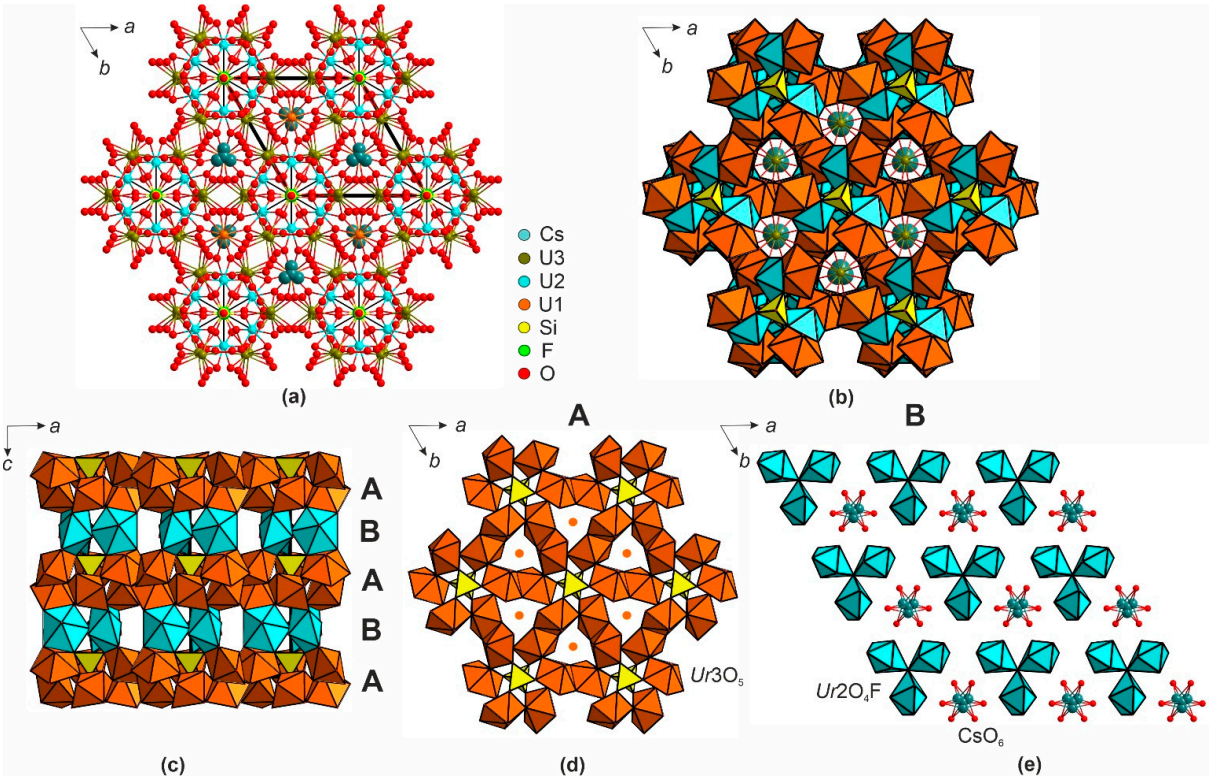

Figure 2. A view of the $Cs[(UO_6)_2(UO_2)_9(Si_2O_7)F]$ structure along the *c* axis in ball-and-stick (**a**) and polyhedral representations (**b**). Projection of **1** onto *ac* plane (**c**); the blocks of **A** (**d**) and **B** (**e**) types can be recognized.

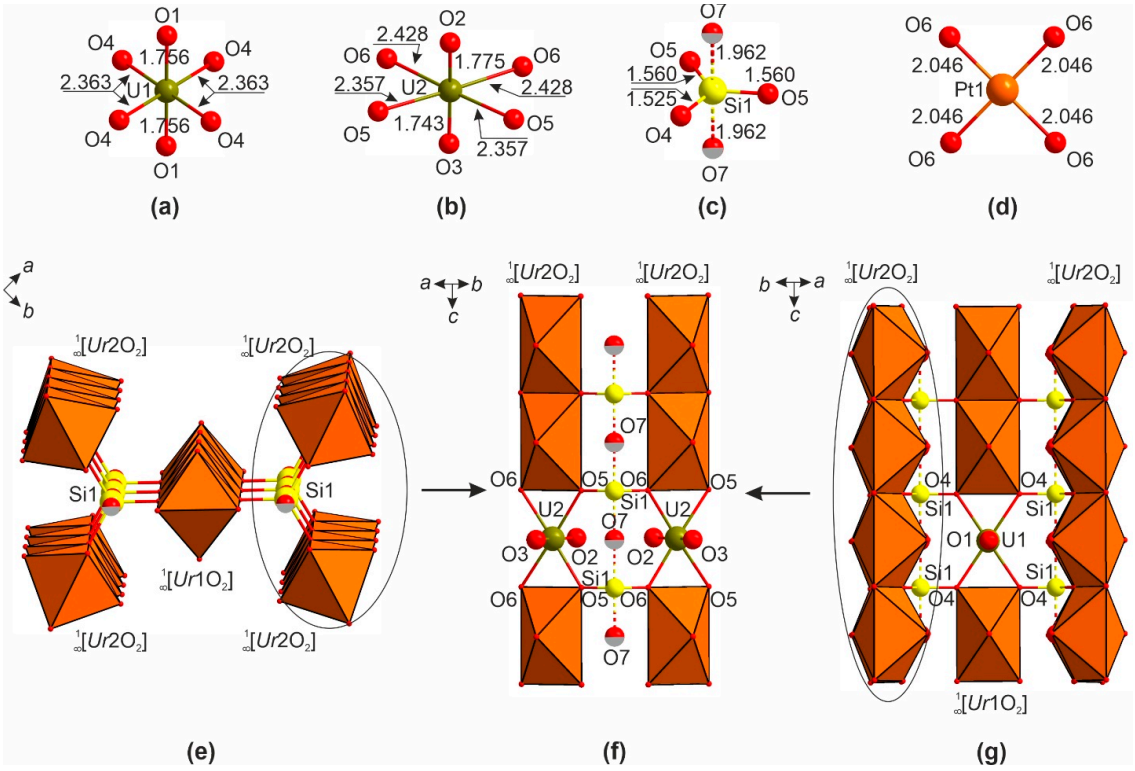

Figure 3. Cation coordination (**a**–**d**) in the structure of $Rb_2[(PtO_4)(UO_2)_5(Si_2O_7)]$. The occupancy of the O7 site is 50%. The $[(UO_2)_5(Si_2O_7)]^{4+}$ chains (**e**). Linkage of the UrO_2 chains via the vertices of the silicate tetrahedra (**f**,**g**).

The platinum site (Figure 3d) is coordinated by four oxygen atoms (<Pt-O> = 2.046 Å) strongly preferred by Pt^{2+}. The bond valence sums (2.24, 6.06, 5.77, 0.97, and 3.78 for Pt1, U1, U2, Rb1, and Si1, respectively), calculated using the parameters from [24], correlated well with the formal valences of the atoms.

The uranium and silicon polyhedra share vertices to form $[(UO_2)_5(Si_2O_7)]^{4+}$ ribbons (Figure 3e). The *Ur*(1)O_4 species share common edges to form the *Ur*(1)O_2 chains, which link to the silicate tetrahedra via the O4 vertex. Similarly, the *Ur*(2)O_4 species share edges to form four *Ur*(2)O_2 chains additionally linked via O5 and O6 oxygens of the silicate units (Figure 3f). Each O5 and O6 vertex therefore belongs to two uranium and one silicon polyhedra. The O7 position is unlikely to be coordinated to the uranium cations. Therefore, each silicon polyhedron is linked to six uranium cations whose coordination mode has not been observed before; the topology of the uranyl-silicate ribbons is also new and unique. These $[(UO_2)_5(Si_2O_7)]^{4+}$ ribbons in **2** are aligned alternatingly (Figure 4) and linked to the framework by the PtO_4 squares. The remaining channels host the rubidium cations.

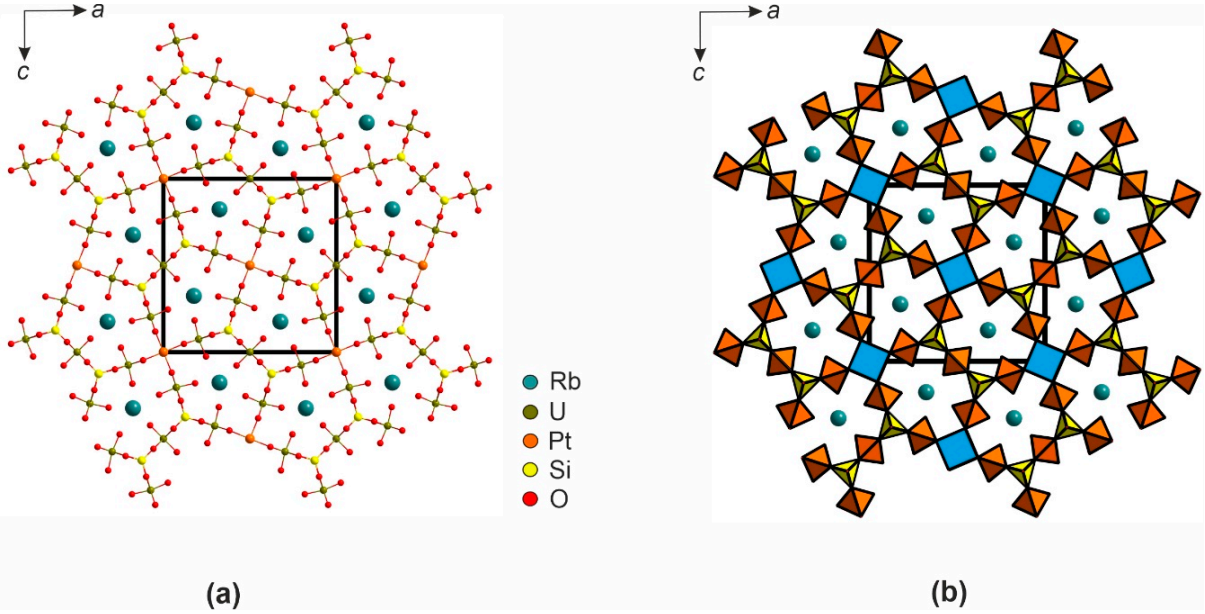

Figure 4. A [010] projection of the structure of **2** in ball-and-stick (**a**) and polyhedral representation (**b**).

4. Discussion

The framework in **1** is structurally close to those in the structures of known uranyl germanates [19]: $NH_4(UO_6)_2[(UO_2)_9(GeO_4)(GeO_3(OH))]$, $K(UO_6)_2[(UO_2)_9(GeO_4)(GeO_3(OH))]$, $Li_3O(UO_6)_2[(UO_2)_9(GeO_4)(GeO_3(OH))]$, and $Ba(UO_6)_2$ $[(UO_2)_9(GeO_4)_2]$. All of these compounds, including **1**, adopt the same space group, and the differences in the cell edges do not exceed 0.2 Å; given these small differences, the metrics of **1** are most close to the Ba uranyl germanate. This is not surprising given that positive differences in the radii of Rb^+ and Ba^{2+} are compensated for by the negative differences in the radii of Si^{4+} and Ge^{4+}. The differences mainly concern the coordination of the tetrahedral cation (Figure 5). In the NH_4, K, and Li compounds, the coordination of germanium is described as trigonal pyramidal so that the chains of such pyramids are stretched along [001]; in addition, one vertex is protonated. Therein, the Ge sites are disordered (Figure 5a), the mean equatorial bond length is 1.695–1.777 Å, and the axial distances range from 1.767 to 2.615 Å.

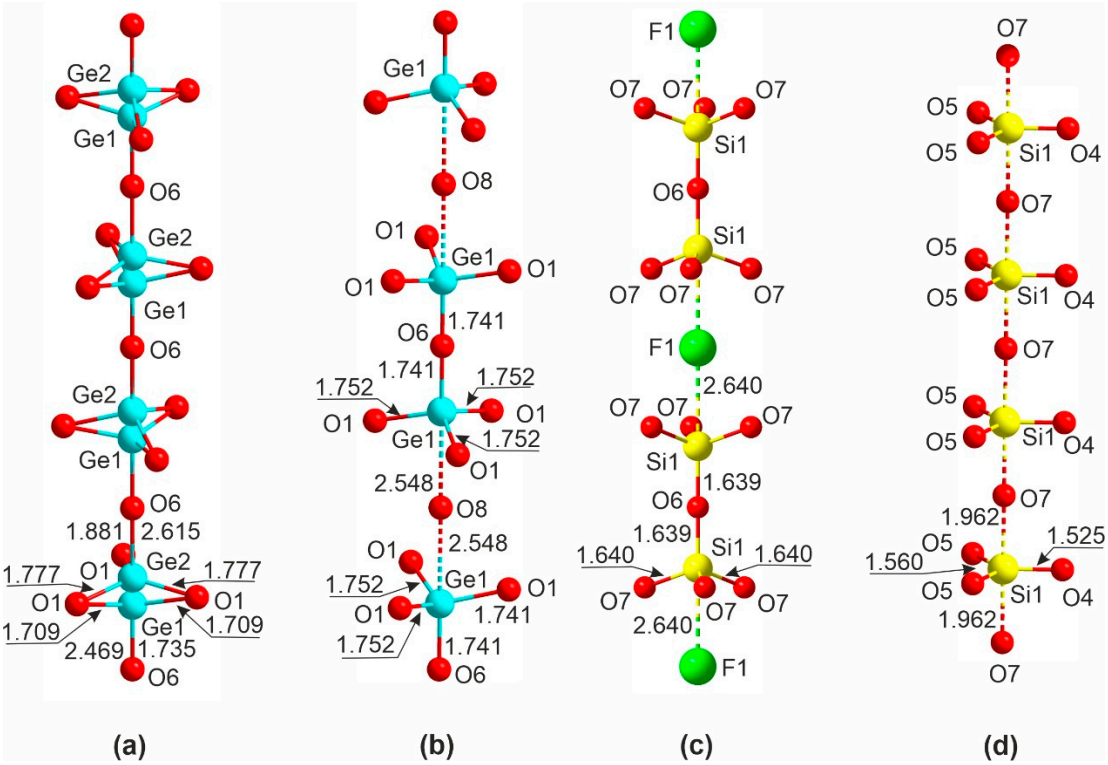

Figure 5. Assemblage of the TO_4 (T = Si, Ge) tetrahedra in the structures of $NH_4(UO_6)_2[(UO_2)_9(GeO_4)(GeO_3(OH))]$; $K(UO_6)_2[(UO_2)_9(GeO_4)(GeO_3(OH))]$; and $Li_3O(UO_6)_2[(UO_2)_9(GeO_4)(GeO_3(OH))]$ (**a**), $Ba(UO_6)_2[(UO_2)_9(GeO_4)_2]$ (**b**), **1** (**c**), and **2** (**d**).

In the structure of $Ba(UO_6)_2[(UO_2)_9(GeO_4)_2]$ (Figure 5b), the germanium sites are ordered so that $[Ge_2O_7]^{6-}$ is clearly visible, and the Ge-O bond lengths range from 1.741–1.752 Å for the terminal oxygens to 2.548 Å for the bridging atoms. A similar pattern is observed for disilicate anion in **1**: the coordination of silicon atoms is a nearly regular tetrahedral with a mean bond length of 1.640(7) Å and O-Si-O angles of 110.6(3) and 108.3(3)°. The F1 sites reside between the disilicate groups; the Si1-F1 separation of 2.640(7) Å (Figure 5c) can be considered nonbonding. In **2** (Figure 5d), the environment of silicon is similar to those of germanium in the structures of uranyl germanates of monovalent cations. As expected, all distances decrease when proceeding from the germanates to the silicate.

Our results illustrate once more that the use of non-ambient conditions is a powerful tool for the preparation of unusual (sometimes even unexpected) compounds. While the preparation of a silicate analog of complex germanates, **1**, does not seem very much surprising, the synthesis of **2** starts a new page in the book of uranium oxide compounds.

By now, there are two compounds containing uranyl cations and platinum, yet the latter is in the state of complex anion, the most common finding in the chemistry of platinum: $K_3((UO_2)_2(OH)(Pt(CN)_4)_2)_2(NO_3)(H_2O)_{1.5}$ [26] and $((U_2(H_2O)_{10}O)(Pt(CN)_4)_3)(H_2O)_4$ [27]. All of the other compounds of U and Pt are oxygen-free intermetallics. We therefore suggest that under conditions close to extreme (high temperatures and pressures, like those in synthesis of **2**), even the platinum metal becomes sufficiently reactive. It is as likely that the simultaneous presence of lead and halide also enhances the reactivity of platinum, maybe via the intermediate formation of its halides: our recent study of the thermal behavior of a $Pb_7O_6Br_2$ oxybromide resulted in the formation of $PbPt_2O_4$ traces above 800 °C [28]. The formation of **2** demonstrates the possibility of preparing other, even less usual, compounds of platinum under severe conditions. On the other hand, structural analogs of **2**, besides the evident replacement of Si by Ge and Rb by Cs or K, may be also obtained using other cations with strongly preferred square planar oxygen coordination, with Pd^{2+} being the

most likely candidate. Square planar coordination is also common for $Cu^{2+,}$ but its geometry is essentially more flexible due to the low crystal field stabilization energy ($3d^9$ configuration). The structure of **2** is also a very rare, if not unique, example of incorporating square planar species into structures of uranyl derivatives with tetrahedral anions. By using appropriate heterovalent substitutions, it is also likely that related architectures can be pursued using other cations with preferred square planar oxide coordination such as Cu^{3+} or Ag^{3+} in oxidizing media or even Ni^{+} in reducing medium. On the other hand, the production of such unusual species can be further enhanced by using noble metal oxides as precursors and strongly oxidizing and basic conditions, as suggested by the successful synthesis of tetravalent platinum borate [29].

5. Conclusions

The new compound **1** is the first example of uranium silicate wherein the uranium polyhedra are linked via cation–cation interactions; it is isostructural to that series of germanium compounds prepared hydrothermally at 220 °C. In contrast, the synthesis of **1** was performed at a higher temperature (900 °C) in evacuated silica tubes, most likely from the melt. As a result, the silicon positions in **1** are fully ordered, and the hydroxide group is replaced by fluorine. Upon the synthesis of **2**, fluoride was not introduced, which resulted, under similar conditions, in the formation of a compound with a poorer order of the silicate sublattice; the most exciting is the incorporation of platinum in positive oxidation state.

Author Contributions: E.V.N., O.I.S. and D.O.C. designed the study, performed, and interpreted single crystal X-ray diffraction experiments; Y.G.T. performed synthesis; and E.V.N., O.I.S., D.O.C. and Y.G.T. wrote the paper. All authors have read and agreed to the published version of the manuscript.

Funding: This research received no external funding.

Institutional Review Board Statement: Not applicable.

Data Availability Statement: The data presented in this study are available on request from the corresponding author.

Acknowledgments: Technical support by the X-ray Diffraction Resource Centre of Saint-Petersburg State University is gratefully acknowledged.

Conflicts of Interest: The authors declare no conflict of interest.

References

1. Belova, L.N.; Doynikova, O.A. Conditions of formation of uranium minerals in the oxidation zone of uranium deposits. *Geol. Ore Deposit* **2003**, *45*, 130–132.
2. Baik, M.H.; Cho, H.R. Roles of uranyl silicate minerals in the long-term mobility of uranium in fractured granite. *J. Radioanal. Nucl. Chem.* **2022**, *331*, 451–459. [CrossRef]
3. Plášil, J. Mineralogy, crystallography and structural complexity of natural uranyl silicates. *Minerals* **2018**, *8*, 551. [CrossRef]
4. Utsunomiya, S.; Ewing, R.C. Radiation-induced decomposition of U(VI) alteration phases of UO_2. *Mater. Res. Soc. Symp. Proceed.* **2006**, *932*, 465–472. [CrossRef]
5. Burns, P.; Olson, R.; Finch, R.; Hanchar, J.; Thibault, Y. $KNa_3(UO_2)_2(Si_4O_{10})_2(H_2O)_4$, a new compound formed during vapor hydration of an actinide-bearing borosilicate *Waste Glass*. *J. Nucl. Mater.* **2000**, *278*, 290–300. [CrossRef]
6. Burns, P.C.; Ewing, R.C.; Miller, M.L. Incorporation mechanisms of actinide elements into the structures of U6+ phases formed during the oxidation of spent nuclear fuel. *J. Nucl. Mater.* **1997**, *245*, 1–9. [CrossRef]
7. Burns, P.C. Cs boltwoodite obtained by ion exchange from single crystals: Implications for radionuclide release in a nuclear repository. *J. Nucl. Mater.* **1999**, *265*, 218–223. [CrossRef]
8. Zolotarev, A.A.; Krivovichev, S.V.; Avdontseva, M.S. Cs-exchanged cuprosklodowskite. In *Minerals as Advanced Materials II*; Springer: Berlin/Heidelberg, Germany, 2012; Volume 2, pp. 163–166.
9. Morrison, G.; Smith, M.D.; Tran, T.T.; Halasyamani, P.S.; Zur Loye, H.C. Synthesis and structure of the new pentanary uranium(vi) silicate, $K_4CaUSi_4O_{14}$, a member of a structural family related to fresnoite. *Cryst. Eng. Comm.* **2015**, *17*, 4218–4224. [CrossRef]
10. Morrison, G.; Zur Loye, H.C. Flux growth of $[NaK_6F][(UO_2)_3(Si_2O_7)_2]$ and $[KK_6Cl][(UO_2)_3(Si_2O_7)_2]$: The effect of surface area to volume ratios on reaction products. *Cryst. Growth Des.* **2016**, *16*, 1294–1299. [CrossRef]
11. Wang, X.; Huang, J.; Liu, L.; Jacobson, A.J. $[(CH_3)_4N][(C_5H_5NH)_{0.8}((CH_3)_3NH)_{0.2}]U_2Si_9O_{23}F_4$ (USH-8): An organically templated open-framework uranium silicate. *J. Mater. Chem.* **2002**, *12*, 406–410. [CrossRef]

12. Liu, H.-K.; Lii, K.-H. $Cs_2USi_6O_{15}$: A tetravalent uranium silicate. *Inorg. Chem.* **2011**, *50*, 5870–5872. [CrossRef] [PubMed]
13. Chen, C.S.; Chiang, R.K.; Kao, H.M.; Lii, K.H. High-temperature, high-pressure hydrothermal synthesis, crystal structure, and solid-state NMR spectroscopy of $Cs_2(UO_2)(Si_2O_6)$ and variable-temperature powder X-ray diffraction study of the hydrate phase $Cs_2(UO_2)(Si_2O_6)\cdot 0.5H_2O$. *Inorg. Chem.* **2005**, *44*, 3914–3918. [CrossRef] [PubMed]
14. Huang, J.; Wang, X.; Jacobson, A.J. Hydrothermal synthesis and structures of the new open-framework uranyl silicates $Rb_4(UO_2)_2(Si_8O_{20})$(USH-2Rb), $Rb_2(UO_2)(Si_2O_6)H_2O$ (USH-4Rb) and $A_2(UO_2)(Si_2O_6)0.5H_2O$ (USH-5A; A = Rb, Cs). *J. Mater. Chem.* **2003**, *13*, 191–196. [CrossRef]
15. Liu, C.-L.; Liu, H.-K.; Chang, W.-J.; Lii, K.-H. $K_2Ca_4[(UO_2)(Si_2O_7)_2]$: A uranyl silicate with a one-dimensional chain structure. *Inorg. Chem.* **2015**, *54*, 8165–8167. [CrossRef] [PubMed]
16. Juillerat, C.A.; Klepov, V.V.; Morrison, G.; Pace, K.A.; Zur Loye, H.C. Flux crystal growth: A versatile technique to reveal the crystal chemistry of complex uranium oxides. *Dalton Trans.* **2019**, *48*, 3162–3181. [CrossRef] [PubMed]
17. Li, H.; Langer, E.M.; Kegler, P.; Alekseev, E.V. Structural and spectroscopic investigation of novel 2D and 3D uranium oxo-silicates/germanates and some statistical aspects of uranyl coordination in oxo-salts. *Inorg. Chem.* **2019**, *58*, 10333–10345. [CrossRef]
18. Fejfarová, K.; Plášil, J.; Yang, H.; Čejka, J.; Dušek, M.; Downs, R.T.; Barkley, M.C.; Škoda, R. Revision of the crystal structure and chemical formula of weeksite, $K_2(UO_2)_2(Si_5O_{13})$ $4H_2O$. *Am. Mineral.* **2012**, *97*, 750–754. [CrossRef]
19. Morrison, J.M.; Moore-Shay, L.J.; Burns, P.C. U(VI) uranyl cation-cation interactions in framework germanates. *Inorg. Chem.* **2011**, *50*, 2272–2277. [CrossRef]
20. Zadoya, A.I.; Siidra, O.I.; Bubnova, R.S.; Nazarchuk, E.V.; Bocharov, S.N. Tellurites of hexavalent uranium: First observation of polymerized $(UO_4)^{2-}$ tetraoxido cores. *Eur. J. Inorg. Chem.* **2016**, *2016*, 4083–4089. [CrossRef]
21. Krot, N.N.; Grigor'ev, M.S. Cation-cation interaction in crystalline actinide compounds. *Uspekhi Khimii.* **2004**, *73*, 94–107.
22. Alekseev, E.V.; Krivovichev, S.V.; Malcherek, T.; Depmeier, W. One-dimensional array of two- and three-center cation-cation bonds in the structure of $Li_4[(UO_2)_{10}O_{10}(Mo_2O_8)]$. *Inorg. Chem.* **2007**, *46*, 8442–8444. [CrossRef] [PubMed]
23. Sheldrick, G.M. Crystal structure refinement with SHELXL. *Acta Crystallogr. Sect. C Struct. Chem.* **2015**, *71*, 3–8. [CrossRef] [PubMed]
24. Gagne, O.C.; Hawthorne, F.C. Bond-length distributions for ions bonded to oxygen: Alkali and alkaline-earth metals. *Acta Crystallogr. Sect B Struct. Sci.* **2016**, *72*, 602–625. [CrossRef]
25. Attfield, M.P.; Catlow, C.R.A.; Sokol, A.A. True structure of trigonal bipyramidal SiO_4F^- species in siliceous zeolites. *Chem. Mater.* **2001**, *13*, 4708–4713. [CrossRef]
26. Maynard, B.A.; Sykora, R.E.; Mague, J.T.; Gorden, A.E.V. Actinide tetracyanoplatinates: Synthesis and structural characterization with uncharacteristic Th-N C coordination and thorium fluorescence. *Chem. Commun.* **2010**, *46*, 4944–4946. [CrossRef] [PubMed]
27. Maynard, B.A.; Lynn, K.S.; Sykora, R.E.; Gorden, A.E.V. Emission, raman spectroscopy, and structural characterization of actinide tetracyanometallates. *Inorg. Chem.* **2013**, *52*, 4880–4889. [CrossRef]
28. Siidra, O.I.; Gogolin, M.; Lukina, E.A.; Kabbour, H.; Bubnova, R.S.; Mentré, O.; Agakhanov, A.A.; Krivovichev, S.V.; Colmont, M.; Gesing, T. Structural evolution from 0D units to 3D frameworks in Pb Oxyhalides: Unexpected strongly corrugated layers in $Pb_7O_6Br_2$. *Inorg. Chem.* **2015**, *54*, 11550–11556. [CrossRef]
29. Hao, Y.; He, L.; Ge, G.; Zhang, Q.; Luo, N.; Huang, S.; Li, H.; Alekseev, E.V. $Mg_3Pt(BO_3)_2O_2$: The first platinum borate from the flux technique. *J. Solid State Chem.* **2020**, *281*, 121046. [CrossRef]